ACS APPLIED MATERIALS & INTERFACES

Research Article

www.acsami.org

Microscopic Dynamics Research on the "Mature" Process of Dye-Sensitized Solar Cells after Injection of Highly Concentrated Electrolyte

Zhongguan Liang,[†] Weiqing Liu,*[,†] Jun Chen,[†] Linhua Hu,[‡] and Songyuan Dai*[,§]

[†]Key Laboratory of Nondestructive Testing, Ministry of Education, School of the Testing and Photoelectric Engineering, Nanchang Hangkong University, Nanchang 330063, P. R. China

[‡]Key Laboratory of Novel Thin-Film Solar Cells, Division of Solar Energy Materials and Engineering, Institute of Plasma Physics, Chinese Academy of Sciences, Hefei 230031, P. R. China

[§]State Key Laboratory of Alternate Electrical Power System with Renewable Energy Sources, North China Electric Power University, Beijing 102206, P. R. China

Supporting Information

ABSTRACT: After injection of electrolyte, the internal three-dimensional solid−liquid penetration system of dye-sensitized solar cells (DSCs) can take a period of time to reach "mature" state. This paper studies the changes of microscopic processes of DSCs including TiO_2 energy-level movement, localized state distribution, charge accumulation, electron transport, and recombination dynamics, from the beginning of electrolyte injection to the time of reached mature state. The results show that the microscopic dynamics process of DSCs exhibited a time-dependent behavior and achieved maturity ∼12 h after injecting the electrolyte into DSCs. Within 0−12 h, several results were observed: (1) the conduction band edge of TiO_2 moved slightly toward negative potential direction; (2) the localized states in the band gap of TiO_2 was reduced according to the same distribution law; (3) the transport resistance in TiO_2 film increased, and electron transport time was prolonged as the time of maturity went on, which indicated that the electron transport process is impeded gradually; (4) the recombination resistance at the TiO_2/electrolyte (EL) interface increases, and electron lifetime gradually extends, therefore, the recombination process is continuously suppressed. Furthermore, results suggest that the parameters of EL/Pt-transparent conductive oxide (TCO) interface including the interfacial capacitance, electron-transfer resistance, and transfer time constant would change with time of maturity, indicating that the EL/Pt-TCO interface is a potential factor affecting the mature process of DSCs.

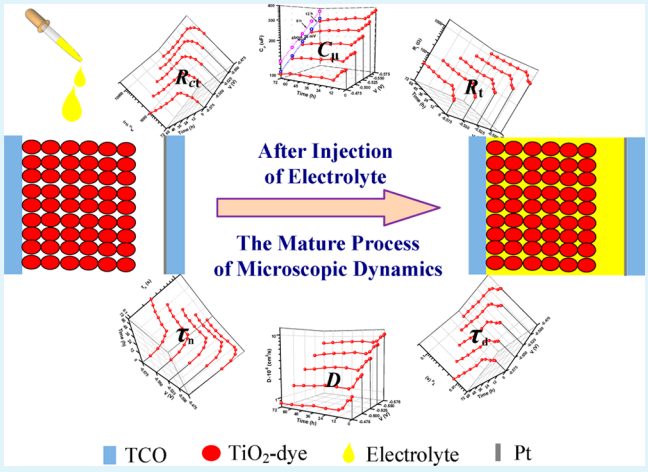

KEYWORDS: *microscopic dynamics, mature process, electrochemical impedance spectroscopy, dye-sensitized solar cell*

1. INTRODUCTION

After decades of research, the highest photoelectric conversion efficiency of dye-sensitized solar cells (DSCs) based on liquid electrolyte has exceeded 12% so far.[1] Typical DSCs consist of transparent conductive oxide (TCO) substrate, nano TiO_2 film, dye, electrolyte (EL), and platinum (Pt). In DSCs, the TCO, TiO_2 film, and dye constitute the photoanode plate and TCO loading Pt constitutes the cathode plate. There is an electrolyte layer between two plates and consequently it is a photo-electrochemical cell with the "sandwich" structure.[2] The following primary steps convert photons to electrical energy that occur in DSCs. After having been excited by a photon, the dye is able to inject an electron to the conduction band of the TiO_2, which is then transported from the injection sites to the TCO/TiO_2 interface. The oxidized dye accepts electrons from the iodide (I^-) in electrolyte leading to regeneration of the ground state. The oxidized redox mediator, triiodide (I_3^-), diffuses toward the EL/Pt-TCO interface, and then it is reduced to I^-. Finally, electrons are collected at the TCO/TiO_2 interface and flow toward the EL/Pt-TCO interface through the external circuit to form a working cycle.[3−5]

Generally speaking, the manufacturing procedure of DSCs can be described as follows: first, form a cavity between photoanode plate and cathode plate through primary seal with a seal ring; second, inject the highly concentrated electrolyte containing various kinds of anion and cation into the cavity;

Received: September 7, 2014
Accepted: December 17, 2014
Published: December 17, 2014

DOI: 10.1021/am506101z
ACS Appl. Mater. Interfaces 2015, 7, 1100−1106

and last, conduct the secondary seal. After injecting electrolyte into the cavity, the photoanode plate and the cathode plate will be immersed into electrolyte forming the three-dimensional solid−liquid penetration system, where the most important microscopic dynamics processes of DSCs occurs.[6] To improve the photovoltaic performance of DSCs, various additives have been added into electrolytes, for example, the commonly used lithium iodide (LiI) and 4-*tert*-butylpyridine (TBP).[7] The high concentration of ions in the electrolyte will significantly influence the photovoltaic performance of DSCs. Li^+ from the electrolyte solution might be intercalated into or adsorbed on the surface of TiO_2 particles,[8,9] which makes the TiO_2 conduction band edge shift to positive potential and raise the efficiency of the photogenerated electron injection from excited dye to TiO_2 conduction band.[10,11] As a result, the photocurrent increased, while open-circuit voltage declined.[12,13] TBP can adsorb on the TiO_2 surface, which makes the TiO_2 conduction band edge shift to negative potential.[14] Meanwhile, TBP constitutes an isolation layer and inhibits the recombination between electron and I_3^-.[15] Both of the action mechanisms of TBP cause the increase of open-circuit voltage of DSCs.

Since the ions need time to reach an adsorption equilibrium on the TiO_2 surface, after injection of electrolyte into the cavity, the device photovoltaic performance, including short-circuit current, open-circuit voltage, fill factor, and conversion efficiency, changes over time and eventually becomes stable. The period from the beginning of electrolyte injection to the time of reached stable state can be called the "mature" process of DSCs. Note that this mature process is different from the "aging" process, which is often seen in some literature. The aging studies focus on the long-term stability of DSCs.[16−20] So far, most studies have ignored the mature period, and, therefore, the microscopic dynamics process causing the change of macroscopic properties during the mature process is still unclear. In this paper, by using the electrochemical impedance spectroscopy (EIS), we conducted multipoint measurements from the beginning of electrolyte injection to the time of reached mature state. This study made an in-depth analysis of the changes of microscopic dynamics on the internal solid/liquid interface of DSCs during the mature process. Furthermore, this study could be helpful for further understanding the electron transport, recombination, and working mechanism of DSCs.

2. EXPERIMENTAL SECTION

Materials. TBP was purchased from Aldrich; iodide (I_2), LiI, 3-methoxypropionitrile (MePN), and 1,2-methyl-3-propylimidazolium iodide (DMPII) were purchased from Fluka, and absolute ethyl alcohol was purchased from Sinopharm Chemical Reagent Beijing Co., Ltd.

Device Fabrication. The colloidal TiO_2 nanoparticles were prepared by hydrolysis of titanium tetraisopropoxide as described elsewhere.[21] The TiO_2 pastes were screen-printed onto the conductive glass (TEC-15, LOF) and sintered in air at 510 °C for 30 min. The thickness of the TiO_2 film was ∼14 μm thick (10 μm thick transparent layer with the particle size of ∼20 nm, and the 4 μm light-scattering layer with the particle size of ∼300−400 nm), and the active area was 0.25 cm^2. At room temperature, the nanoporous TiO_2 photoelectrodes were immersed in an ethanol solution of 0.5 mM N719 dye for 12 h. The Pt-TCO counter electrodes were obtained by spraying H_2PtCl_6 solution on TCO and sintered at 410 °C for 20 min. DSCs were assembled by sealing the dye-loaded TiO_2 photoelectrode and the Pt-TCO counter electrode with a 60 μm thermal adhesive film (Surlyn, Dupont). The electrolyte (composed of 0.5 M TBP, 0.1 M LiI, 0.08 M I_2, and 0.6 M DMPII in the solvent of MePN) was injected into the cavity between the two electrodes through a hole on the counter electrode, and the hole was later sealed with a cover glass and thermal adhesive film. Pt−Pt symmetrical cell was assembled by two Pt-TCO electrodes and injection of the same electrolyte.

Measurements. The photovoltaic performance of DSCs with the active area of 0.25 cm^2 was measured by using a Keithley 2420 digital source meter (Keithley, USA) and was controlled using Text point software under a 450 W xenon lamp (Orial, U.S.A.) with a filter (AM 1.5, 100 mW/cm^2). The incident light intensity was calibrated with a standard crystalline silicon solar cell before each experiment. EIS measurements were performed on an electrochemical workstation (IM6ex, German Zahner Company), at perturbation amplitude of 10 mV within the frequency range from 1 MHz to 80 mHz in the dark. This batch of DSCs was divided into two groups that were then used for *I*−*V* and EIS measurements, respectively. The cells were measured at the time points of 0, 1, 4, 8, 12, 24, 36, 48, 60, and 72 h after fabrication. Beyond measurement time, the cells were placed in an indoor environment in the dark. The impedance parameters information on DSCs were extracted using transmission line model.[22,23] The impedance parameters information on Pt−Pt symmetrical cells were extracted using the equivalent circuit mentioned in literature.[24]

3. RESULTS AND DISCUSSION

To understand the mature process of DSCs, the changes of photovoltaic parameters of cells under AM 1.5 irradiation of 100 mW/cm^2 were obtained (see Supporting Information, Figure S1). It was found that short-circuit current (J_{sc}) gradually decreased within 0−12 h as mature time goes on. Open-circuit voltage (V_{oc}) and fill factor (FF), however, gradually increased in this period, and finally led to an increase in conversion efficiency (η). After 12 h, all photovoltaic parameters changed slightly.

Several interfaces formed due to internal two-phase contact in "sandwich"-type DSCs: (1) the interface between TiO_2 film and TCO (TiO_2/TCO interface); (2) the interface between TiO_2 film and electrolyte (TiO_2/EL interface); (3) the interface between electrolyte and Pt-TCO counter electrode (EL/Pt-TCO interface); and (4) the interface between TCO and electrolyte (TCO/EL interface).[6] EIS is a very powerful method for studying various interfacial processes. When the applied bias voltage changed, EIS would show different interface impedance characteristics in various frequency ranges.[25,26] Figure S2 in the Supporting Information shows the Nyquist plots obtained in the dark under a bias of −0.575 V. In the high-frequency range, the first semicircle corresponds to the impedance information on charge-transfer process at EL/Pt-TCO interface. With gradually reducing frequency, the second semicircle in the medium-frequency range corresponds to charge recombination process at TiO_2/EL interface. As shown in the Nyquist plots, the second semicircle gradually enlarged within 0−12 h. The changes of the impedance are mainly concentrated in 0−12 h, and that result is consistent with the changes of the photovoltaic parameters.

3.1. Changes of Localized Electronic States during the Mature Process. Studies show that localized states with exponential distribution play different roles during the photoelectric conversion process: (1) the localized states in the bulk affects the transport and recombination process of the free electron in the conduction band through the trapping/detrapping effect; (2) the localized states on the particle surface can be involved in the recombination process.[27,28] The changes of Fermi level can cause changes of electron density in the corresponding states. In this case, a parameter, namely, chemical capacitance (C_μ), can be defined.[28−30] The chemical

DOI: 10.1021/am506101z
ACS Appl. Mater. Interfaces 2015, 7, 1100−1106

capacitance of TiO_2 film can directly reflect the distribution of localized states.[31] The relationship between C_μ and applied bias voltage (V) is shown as follows.[31]

$$C_\mu = C_0 \exp\left[\frac{\alpha q}{k_B T} V\right] = C_0 \exp\left[\frac{q}{k_B T_0} V\right] \quad (1)$$

where C_0 is a constant, q is the elementary charge, k_B is Boltzmann's constant, T is temperature, T_0 is characteristic temperature, and $\alpha = T/T_0$, which is the dimensionless constant, representing the depth of the distribution of localized state. T_0 of localized states in the bulk and at the particle surface of TiO_2 may be different or same. Here, assume that these T_0 values are the same. So, eq 1 shows the total density of localized states with exponential distribution in the TiO_2 band gap.

Figure 1 shows the changes of chemical capacitance with the applied bias voltage during the mature time. Under the same

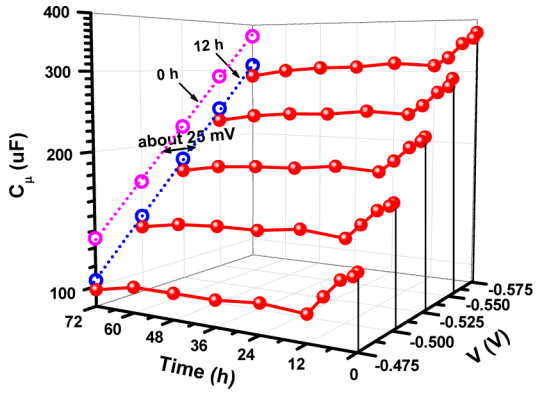

Figure 1. Changes of chemical capacitance with the applied bias voltage during the mature time. Taking the capacitance at 0 h as reference, a negative potential shift of ~25 mV is observed as mature time goes from 0 to 12 h.

bias voltage, C_μ gradually decreases within 0−12 h as mature time goes on, and decreases slowly after 12 h. At the same time point, C_μ increases exponentially with the applied negative bias voltage increases.

The α values varying with mature time were obtained by fitting the relationship between C_μ and V in Figure 1 through eq 1 and are shown in Figure 2. The α value almost remains unchanged as mature time goes on, indicating that the distribution of localized states of TiO_2 does not change. Because of the huge surface area of mesoporous TiO_2 film, localized states may be mainly located at the particle surface. During the mature process, chemical capacitance became smaller as time goes on, which is probably induced by the adsorption of ions. It causes the change of localized states on the TiO_2 surface after electrolyte injection. Our study results show that the quantity of localized states decreases according to the same distribution law.

If sufficient charges are accumulated on the TiO_2 surface, the potential drop in Helmholtz layer may be changed. It causes the conduction band edge movement. When the surface accumulates positive charge, the conduction band edge will shift to the positive potential; when the surface accumulates negative charge, the conduction band edge will shift to the negative potential.[32] According to the relationship between C_μ and V as shown in Figure 1, taking the capacitance at 0 h as reference, the conduction band edge of TiO_2 shifts by ~25 mV to the

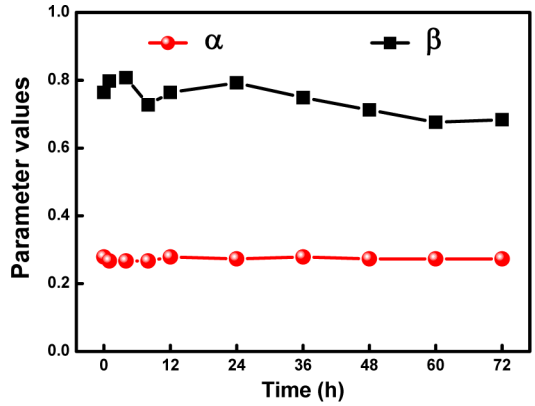

Figure 2. Values of α and β varying with mature time. α is a dimensionless constant that ranges from 0 to 1. One can get information by using eq 1, representing the depth of the distribution of localized state. β also is a dimensionless constant that ranges from 0 to 1. One can get information by using eq 4, representing the recombination reaction order.

negative potential as mature time goes from 0 to 12 h. Because of adsorption of Li^+, that TiO_2 conduction band edge shifts to the positive potential, while the introduction of TBP into the electrolyte can make TiO_2 conduction band shift to the negative potential. Some studies have shown that TBP could reduce positive charge density of TiO_2 surface.[33,34] In this study, TiO_2 conduction band edge eventually shifts toward negative potential direction, indicating that TBP plays a dominant role in the movement of conduction band edge of TiO_2 as mature time goes on.

3.2. Changes of Transport during the Mature Process.

Electron transport through the mesoporous TiO_2 film usually suffers some drags, which can be equivalent to the charge transport resistance.[22] Figure 3 shows the changes of electron

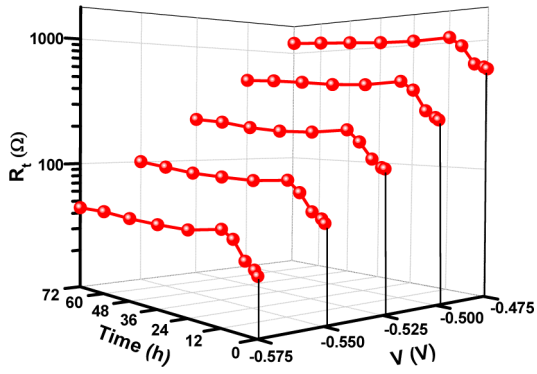

Figure 3. Changes of transport resistance with the applied bias voltage during the mature time.

transport resistance (R_t) with the applied bias voltage during the mature time. The R_t gradually increases during 0−12 h under the same bias voltage, indicating that the drag of electron transport gradually increases, but increases slightly after 12 h. The relationship between the transport resistance and the applied bias voltage is expressed as follows.[22]

$$R_t = R_0 \exp\left[-\frac{q}{k_B T}\left(V + \frac{E_{F,redox} - E_c}{q}\right)\right] \quad (2)$$

DOI: 10.1021/am506101z
ACS Appl. Mater. Interfaces 2015, 7, 1100−1106

where R_0 is a constant, E_c is the conduction band energy level, and $E_{F,redox}$ is the redox potential. At the same time points, R_t decreased exponentially with the applied negative bias voltage increases.

In DSCs, electrons transport by diffusion through mesoporous TiO_2 film, and this can be characterized by diffusion coefficient (D)[35] as follows.

$$D = \frac{L^2}{\tau_d} \tag{3}$$

where L is the thickness of TiO_2 film. The transit time of electron across the TiO_2 film is obtained by $\tau_d = R_t \cdot C_\mu$.[36,37] Equation 3 indicates that under the same thickness, the higher diffusion coefficient means that the electrons can reach the conductive substrate in a shorter time. Figures 4 and 5 show the

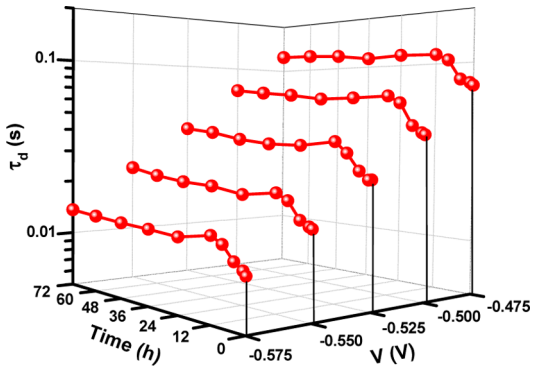

Figure 4. Changes of transit time with the applied bias voltage during the mature time.

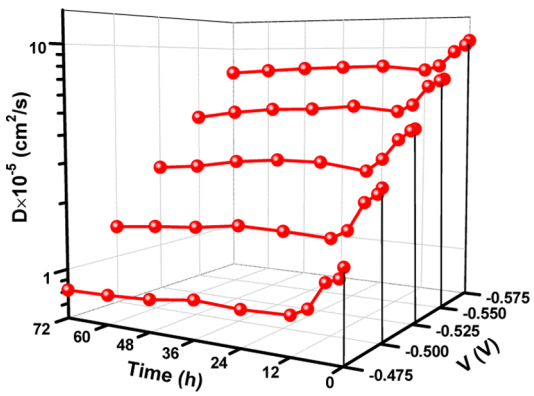

Figure 5. Changes of diffusion coefficient with the applied bias voltage during the mature time.

changes of transit time and diffusion coefficient with the applied bias voltage during the mature time, respectively. Results show that under the same bias voltage, the transit time gradually prolonges as the mature time goes on during 0−12 h, indicating that electron transport was hindered, but the change of electron transit time became stable after 12 h. The diffusion coefficient gradually decreases, which shows that the diffusion of electron was hindered during the mature time.

The exponential relationship between the transit time and the applied bias voltage can be interpreted through the Multiple-Trapping model.[38] Because of the localized states with exponential distribution below the conduction band, electron transport in the conduction band will be affected by trapping/detrapping process. When the Fermi level is lower, the trapping/detrapping effect will become larger. With the rise of the Fermi level, the localized states will be filled gradually, and the impact of the trapping/detrapping will be gradually reduced.

Kopidakis et al. found that intercalation of Li^+ into TiO_2 nanoparticle layer in DSCs increased charge transport time constants.[39] Wang and co-workers[40] report a very interesting result that proposed a new mechanism about Li^+ as additives in DSCs. They found the formation of shallow trapping states close to the conduction band resulted most likely from photoinduced proton intercalation in the TiO_2 nanoparticles under visible-light soaking, which can accelerate the charge-carrier transport within the films. But the introduction of Li^+ in the electrolyte suppresses the phenomena due to prevailing Li^+ intercalation. Since our cells are not illuminated by strong light, Li^+ may not be intercalated deeply into the TiO_2 nanoparticle, but, at least, Li^+ may be intercalated very shallowly or adsorbed at the surface. Because of the huge surface area of mesoporous TiO_2 film, it should be possible to achieve a sufficient amount to change the electron transport process. Chemical adsorption of TBP on the TiO_2 surface may affect the electron transport process. The neck part between the two adjacent TiO_2 particles might also affect the overall electron transport.[41,42] In addition, TBP might form a blocking layer in the neck part between the two adjacent TiO_2 particles, which is very likely to become a factor hindering electron transport.

Electron injection efficiency is affected by the movement of conduction band edge. TiO_2 conduction band edge shifts eventually toward the negative potential direction (Figure 1), so electron injection efficiency is suppressed. Consequently, the electron transport driving force was affected. As a result, it is reasonable to conclude that the J_{sc} decreases may be explained by the markedly slower electron transport and the lower electron injection efficiency as mature time goes on.

3.3. Changes of Recombination during the Mature Process. Recombination is an important factor affecting the conversion efficiency of DSCs. Recombination in DSCs is a process of interface transfer, which occurs only at the interface.[43] On the TiO_2/EL interface, photogenerated electrons can recombine with the excited-state dye or I_3^- in the solution.[5,44] TCO/EL interface is also involved in the recombination process, especially when the DSCs use the fast redox couple[45] or the solid electrolyte.[46] Recombination at the TCO/EL interface will influence the cell photovoltaic performance significantly. The electron recombination reaction is characterized by recombination resistance (R_{ct}). A larger R_{ct} value means that the recombination reaction more difficultly occurs between electrons and acceptor in electrolyte.[4] The most important recombination for DSCs is that of TiO_2 electrons and I_3^- ions through the TiO_2/EL interface.

Figure 6 shows the changes of electron recombination resistance at the TiO_2/EL interface with the applied bias voltage during the mature time. Under the same bias voltage, R_{ct} gradually increases as time goes on within 0−12 h but changed slightly after 12 h. At the same time points, R_{ct} would exponentially decrease with the increase of the applied bias voltage.

The relationship between the recombination resistance and voltage is described as follows.[22]

DOI: 10.1021/am506101z
ACS Appl. Mater. Interfaces 2015, 7, 1100−1106

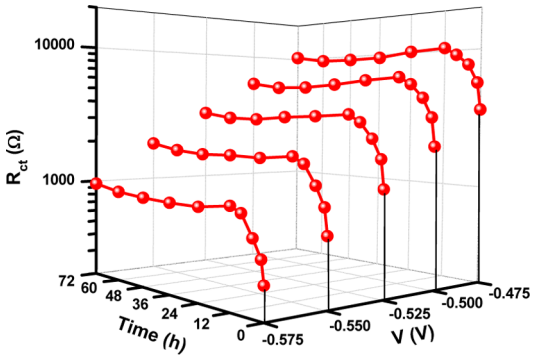

Figure 6. Changes of recombination resistance with the applied bias voltage during the mature time.

$$R_{ct} = A\exp\left[-\frac{\beta q}{k_B T}V\right] \quad (4)$$

where A is a constant, and β is a dimensionless constant, representing the recombination reaction order, which ranges from 0 to 1. Recombination reaction of electrons on the TiO_2/EL interface is achieved mainly through two ways:[32,47] (1) directly recombine with I_3^- ions in the electrolyte through the TiO_2 conduction band; (2) indirectly recombine with I_3^- ions in the electrolyte through the surface states. When $\beta = 1$, electron recombination mainly occurs through the conduction band; in more cases $\beta < 1$, and electron recombination occurs via the surface states.[7,48,49] By fitting the relationship between R_{ct} and V in Figure 6 through eq 4, the β value at various measurement time points can be obtained (Figure 2). From Figure 2, β becomes slightly smaller as mature time goes on but is always less than 1, indicating that the way of electron recombination does not change and that electron recombination happens mainly through surface states during the whole mature process. The recombination process was suppressed probably because recombination sites on the TiO_2 surface decreases with the adsorption of TBP.[15]

The electron lifetime $\tau_n = R_{ct}\cdot C_\mu$ can be used to characterize the recombination reaction kinetics.[37] Figure 7 shows the changes of electron lifetime with the applied bias voltage during the mature time. Under the same bias voltage within 0−12 h, electron lifetime prolonged continuously as time goes on. Kopidakis and co-workers[39] performed transport and recombination studies, and the results have shown that the transport process limits the recombination process. The relationship between τ_d and τ_n could described with a simple formula.

$$\tau_d \propto \frac{1}{D} \propto \tau_n \quad (5)$$

where τ_d represents the transport process, and τ_n represents the recombination process. Equation 5 implies that a change in the electron transit time results in the corresponding change of electron lifetime. So, we could reasonably infer that the τ_n increases may be due to the electron transport-limited recombination process. As shown in Figure 4, the τ_d increases mean that electron transport slowed and that the probability of meeting the electron acceptor in the electrolyte was reduced. Finally, it resulted in the corresponding extension of electron lifetime. Therefore, the gradual V_{oc} enhancement during 0−12 h could be due to the suppressed recombination, which can be attributed mainly to TBP molecules gradually adsorption on the TiO_2 surface as time goes on.

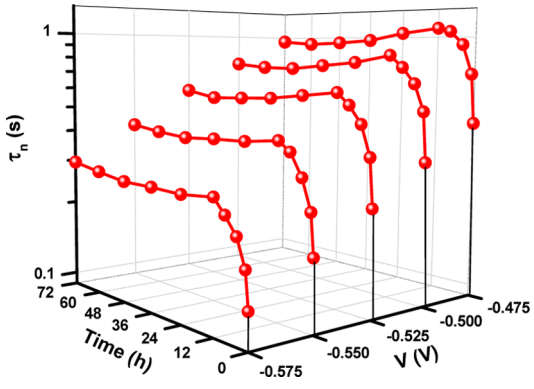

Figure 7. Changes of electron lifetime with the applied bias voltage during the mature time.

3.4. Changes of EL/Pt-TCO Interface during the Mature Process. To understand the effect of EL/Pt-TCO interface on the mature process, this study includes measurements of the impedance variation of Pt−Pt symmetric cells through EIS during the mature period.

EL/Pt-TCO interface capacitance may be mainly the Helmholtz capacitance.[31,50] Figure 8 shows the changes of EL/Pt-TCO interface capacitance with the applied bias voltage during the mature time. After injection of electrolyte, EL/Pt-TCO interface capacitance decreases slightly within 0−12 h. The possible reason is that the ionic adsorption affects the charge amount of double electric layers and thus results in changes of interface capacitance.

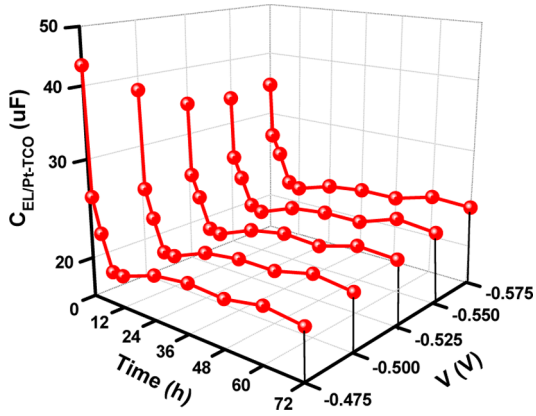

Figure 8. Changes of EL/Pt-TCO interface capacitance with the applied bias voltage during the mature time.

Figures 9 and 10 show the changes of EL/Pt-TCO interface transfer resistance ($R_{EL/Pt\text{-}TCO}$) and transfer time constant ($\tau_{EL/Pt\text{-}TCO}$) with the change of applied bias voltage during the mature time, respectively. $R_{EL/Pt\text{-}TCO}$ increases gradually with mature time goes on within 0−12 h, maybe because of adsorption of Li^+ and TBP at the EL/Pt-TCO interface. The reduction of EL/Pt-TCO interface capacitance finally resulted in the decreases of time constant $\tau_{EL/Pt\text{-}TCO}$, which was illustrated in Figure 10, indicating that the electron transfer rate of EL/Pt-TCO interface has some improvement. The above results show that the relevant electrochemical performance of EL/Pt-TCO interface also needs to be considered during the mature process.

DOI: 10.1021/am506101z
ACS Appl. Mater. Interfaces 2015, 7, 1100−1106

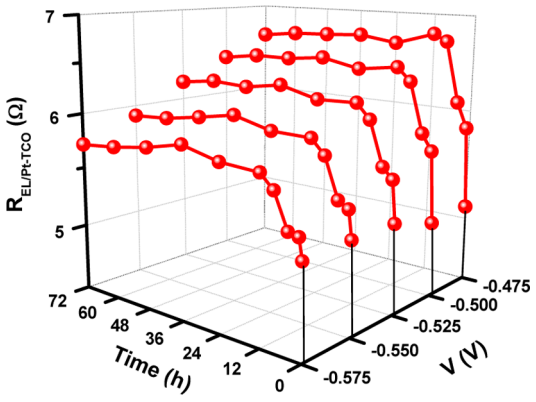

Figure 9. Changes of EL/Pt-TCO interface transfer resistance with the applied bias voltage during the mature time.

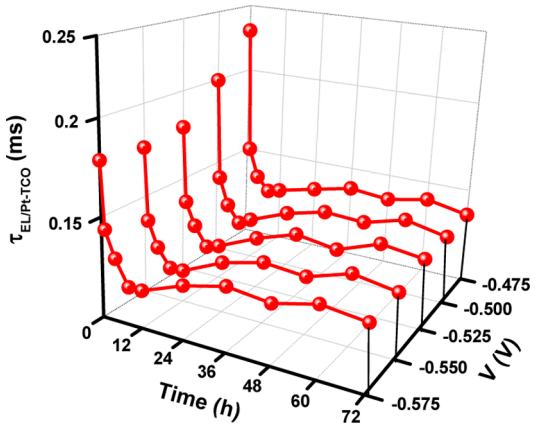

Figure 10. Changes of EL/Pt-TCO interface transfer time constant with the applied bias voltage during the mature time.

4. CONCLUSIONS

In conclusion, we studied the changes of microscopic processes of DSCs including TiO_2 energy level movement, localized states distribution, charge accumulation, electron transport, and recombination dynamics, from the beginning of electrolyte injection to the mature state. Our results showed that the microscopic parameters exhibited a time-dependent behavior. It is found that the microscopic dynamics process of DSCs achieved mature state after ~12 h when the electrolyte was injected. Within 0−12 h, we can conclude that (1) the adsorption of ions on the TiO_2 surface resulted in a slight shift of TiO_2 conduction band edge to negative potential; (2) the localized states in the band gap of TiO_2 reduced according to the same distribution law; (3) the electron transport resistance in TiO_2 film increased, and electron transport time prolonged as time went on, while the electron diffusion coefficient continuously decreased, which indicated that the electron transport process slowed down; (4) the recombination resistance at the TiO_2/EL interface increased, and the electron lifetime gradually prolonged over time, therefore, the recombination process was continuously suppressed. The changes of the *I*−*V* parameters are mainly concentrated in 0−12 h, which is consistent with the changes over time of the microscopic parameters measured by EIS. In addition, our results suggest that the parameters of EL/Pt-TCO interface including the interface capacitance, transfer resistance, and transfer time constant also changed with the mature time, indicating that this interface is a potential factor affecting the mature process of DSCs.

■ ASSOCIATED CONTENT

Supporting Information

Additional macroscopic photovoltaic information and the Nyquist plot of the DSCs. This material is available free of charge via the Internet at http://pubs.acs.org.

■ AUTHOR INFORMATION

Corresponding Authors

*E-mail: peizheni@163.com. (W.L.)
*E-mail: sydai@ipp.ac.cn. (S.D.)

Notes

The authors declare no competing financial interest.

■ ACKNOWLEDGMENTS

This work was financially supported by the National Basic Research Program of China under Grant No. 2011CBA00700, the National Natural Science Foundation of China under Grant No. 11464029, the China Postdoctoral Science Foundation Funded Project under Grant Nos. 20110490835 and 2012T50581, and the Graduate Innovation Special Fund Project of Jiangxi Province under Grant No.YC2013-S213.

■ REFERENCES

(1) Mathew, S.; Yella, A.; Gao, P.; Humphry-Baker, R.; Curchod, B. F. E.; Ashari-Astani, N.; Tavernelli, I.; Rothlisberger, U.; Nazeeruddin, M. K.; Grätzel, M. Dye-Sensitized Solar Cells with 13% Efficiency Achieved Through the Molecular Engineering of Porphyrin Sensitizers. *Nat. Chem.* **2014**, *6*, 242−247.

(2) O'Regan, B.; Grätzel, M. A Low-Cost, High-Efficiency Solar Cell Based on Dye-Sensitized Colloidal TiO_2 Films. *Nature* **1991**, *353*, 737−740.

(3) Schwarzburg, K.; Willig, F. Origin of Photovoltage and Photocurrent in the Nanoporous Dye-Sensitized Electrochemical Solar Cell. *J. Phys. Chem. B* **1999**, *103*, 5743−5746.

(4) Peter, L. M. Dye-Sensitized Nanocrystalline Solar Cells. *Phys. Chem. Chem. Phys.* **2007**, *9*, 2630−2642.

(5) Hagfeldt, A.; Lindquist, S. E.; Grätzel, M. Charge-Carrier Separation and Charge-Transport in Nanocrystalline Junctions. *Sol. Energy Mater. Sol. Cells* **1994**, *32*, 245−257.

(6) Liu, W. Q.; Liang, Z. G.; Kou, D. X.; Hu, L. H.; Dai, S. Y. Wide Frequency Range Diagnostic Impedance Behavior of the Multiple Interfaces Charge Transport and Transfer Processes in Dye-Sensitized Solar Cells. *Electrochim. Acta* **2013**, *88*, 395−403.

(7) Idígoras, J. s.; Pellejà, L.; Palomares, E.; Anta, J. A. The Redox Pair Chemical Environment Influence on the Recombination Loss in Dye-Sensitized Solar Cells. *J. Phys. Chem. C* **2014**, *118*, 3878−3889.

(8) Zaban, A.; Meier, A.; Gregg, B. A. Electric Potential Distribution and Short-Range Screening in Nanoporous TiO_2 Electrodes. *J. Phys. Chem. B* **1997**, *101*, 7985−7990.

(9) Södergren, S.; Siegbahn, H.; Rensmo, H.; Lindström, H.; Hagfeldt, A.; Lindquist, S.-E. Lithium Intercalation in Nanoporous Anatase TiO_2 Studied with XPS. *J. Phys. Chem. B* **1997**, *101*, 3087−3090.

(10) Haque, S. A.; Palomares, E.; Cho, B. M.; Green, A. N.; Hirata, N.; Klug, D. R.; Durrant, J. R. Charge Separation Versus Recombination in Dye-Sensitized Nanocrystalline Solar Cells: The Minimization of Kinetic Redundancy. *J. Am. Chem. Soc.* **2005**, *127*, 3456−3462.

(11) Tachibana, Y.; Haque, S. A.; Mercer, I. P.; Moser, J. E.; Klug, D. R.; Durrant, J. R. Modulation of the Rate of Electron Injection in Dye-Sensitized Nanocrystalline TiO_2 Films by Externally Applied Bias. *J. Phys. Chem. B* **2001**, *105*, 7424−7431.

DOI: 10.1021/am506101z
ACS Appl. Mater. Interfaces 2015, 7, 1100−1106

(12) Kelly, C. A.; Farzad, F.; Thompson, D. W.; Stipkala, J. M.; Meyer, G. J. Cation-Controlled Interfacial Charge Injection in Sensitized Nanocrystalline TiO_2. *Langmuir* **1999**, *15*, 7047−7054.
(13) Pelet, S.; Moser, J.-E.; Grätzel, M. Cooperative Effect of Adsorbed Cations and Iodide on the Interception of Back Electron Transfer in the Dye Sensitization of Nanocrystalline TiO_2. *J. Phys. Chem. B* **2000**, *104*, 1791−1795.
(14) Boschloo, G.; Häggman, L.; Hagfeldt, A. Quantification of the Effect of 4-tert-Butylpyridine Addition to I^-/I_3^- Redox Electrolytes in Dye-Sensitized Nanostructured TiO_2 Solar Cells. *J. Phys. Chem. B* **2006**, *110*, 13144−13150.
(15) Dürr, M.; Yasuda, A.; Nelles, G. On the Origin of Increased Open Circuit Voltage of Dye-Sensitized Solar Cells Using 4-tert-Butylpyridine as Additive to the Electrolyte. *Appl. Phys. Lett.* **2006**, *89*, 061110.
(16) Hinsch, A.; Kroon, J.; Kern, R.; Uhlendorf, I.; Holzbock, J.; Meyer, A.; Ferber, J. Long-Term Stability of Dye-Sensitised Solar Cells. *Prog. Photovoltaics* **2001**, *9*, 425−438.
(17) Yum, J.-H.; Humphry-Baker, R.; Zakeeruddin, S. M.; Nazeeruddin, M. K.; Grätzel, M. Effect of Heat and Light on the Performance of Dye-Sensitized Solar Cells Based on Organic Sensitizers and Nanostructured TiO_2. *Nano Today* **2010**, *5*, 91−98.
(18) Kuang, D.; Wang, P.; Ito, S.; Zakeeruddin, S. M.; Grätzel, M. Stable Mesoscopic Dye-Sensitized Solar Cells Based on Tetracyanoborate Ionic Liquid Electrolyte. *J. Am. Chem. Soc.* **2006**, *128*, 7732−7733.
(19) Pettersson, H.; Gruszecki, T. Long-Term Stability of Low-Power Dye-Sensitised Solar Cells Prepared by Industrial Methods. *Sol. Energy Mater. Sol. Cells* **2001**, *70*, 203−212.
(20) Fei, Z. F.; Kuang, D. B.; Zhao, D. B.; Klein, C.; Ang, W. H.; Zakeeruddin, S. M.; Gratzel, M.; Dyson, P. J. A Supercooled Imidazolium Iodide Ionic Liquid as a Low-Viscosity Electrolyte for Dye-Sensitized Solar Cells. *Inorg. Chem.* **2006**, *45*, 10407−10409.
(21) Hu, L. H.; Dai, S. Y.; Weng, J.; Xiao, S. F.; Sui, Y. F.; Huang, Y.; Chen, S. H.; Kong, F. T.; Pan, X.; Liang, L. Y.; Wang, K. J. Microstructure Design of Nanoporous TiO_2 Photoelectrodes for Dye-Sensitized Solar Cell Modules. *J. Phys. Chem. B* **2007**, *111*, 358−362.
(22) Fabregat-Santiago, F.; Bisquert, J.; Garcia-Belmonte, G.; Boschloo, G.; Hagfeldt, A. Influence of Electrolyte in Transport and Recombination in Dye-Sensitized Solar Cells Studied by Impedance Spectroscopy. *Sol. Energy Mater. Sol. Cells* **2005**, *87*, 117−131.
(23) Bisquert, J.; Gratzel, M.; Wang, Q.; Fabregat-Santiago, F. Three-Channel Transmission Line Impedance Model for Mesoscopic Oxide Electrodes Functionalized with a Conductive Coating. *J. Phys. Chem. B* **2006**, *110*, 11284−11290.
(24) Hauch, A.; Georg, A. Diffusion in the Electrolyte and Charge-Transfer Reaction at the Platinum Electrode in Dye-Sensitized Solar Cells. *Electrochim. Acta* **2001**, *46*, 3457−3466.
(25) Wang, Q.; Moser, J. E.; Gratzel, M. Electrochemical Impedance Spectroscopic Analysis of Dye-Sensitized Solar Cells. *J. Phys. Chem. B* **2005**, *109*, 14945−14953.
(26) Han, L.; Koide, N.; Chiba, Y.; Islam, A.; Mitate, T. Modeling of an Equivalent Circuit for Dye-Sensitized Solar Cells: Improvement of Efficiency of Dye-Sensitized Solar Cells by Reducing Internal Resistance. *C. R. Chim.* **2006**, *9*, 645−651.
(27) Ondersma, J. W.; Hamann, T. W. Measurements and Modeling of Recombination from Nanoparticle TiO_2 Electrodes. *J. Am. Chem. Soc.* **2011**, *133*, 8264−8271.
(28) Bisquert, J.; Zaban, A.; Greenshtein, M.; Mora-Sero, I. Determination of Rate Constants for Charge Transfer and the Distribution of Semiconductor and Electrolyte Electronic Energy Levels in Dye-Sensitized Solar Cells by Open-Circuit Photovoltage Decay Method. *J. Am. Chem. Soc.* **2004**, *126*, 13550−13559.
(29) Bisquert, J. Chemical Capacitance of Nanostructured Semiconductors: Its Origin and Significance for Nanocomposite Solar Cells. *Phys. Chem. Chem. Phys.* **2003**, *5*, 5360−5364.
(30) Pascoe, A. R.; Bourgeois, L.; Duffy, N. W.; Xiang, W.; Cheng, Y.-B. Surface State Recombination and Passivation in Nanocrystalline TiO_2 Dye-Sensitized Solar Cells. *J. Phys. Chem. C* **2013**, *117*, 25118−25126.
(31) Wang, Q.; Ito, S.; Grätzel, M.; Fabregat-Santiago, F.; Mora-Sero, I.; Bisquert, J.; Bessho, T.; Imai, H. Characteristics of High Efficiency Dye-Sensitized Solar Cells. *J. Phys. Chem. B* **2006**, *110*, 25210−25221.
(32) Schlichthorl, G.; Huang, S. Y.; Sprague, J.; Frank, A. J. Band Edge Movement and Recombination Kinetics in Dye-Sensitized Nanocrystalline TiO_2 Solar Cells: A Study by Intensity Modulated Photovoltage Spectroscopy. *J. Phys. Chem. B* **1997**, *101*, 8141−8155.
(33) Nakade, S.; Kanzaki, T.; Kubo, W.; Kitamura, T.; Wada, Y.; Yanagida, S. Role of Electrolytes on Charge Recombination in Dye-Sensitized TiO_2 Solar Cell (1): The Case of Solar Cells Using the I^-/I_3^- Redox Couple. *J. Phys. Chem. B* **2005**, *109*, 3480−3487.
(34) Katoh, R.; Kasuya, M.; Kodate, S.; Furube, A.; Fuke, N.; Koide, N. Effects of 4-*tert*-Butylpyridine and Li Ions on Photoinduced Electron Injection Efficiency in Black-Dye-Sensitized Nanocrystalline TiO_2 Films. *J. Phys. Chem. C* **2009**, *113*, 20738−20744.
(35) Bisquert, J. Chemical Diffusion Coefficient of Electrons in Nanostructured Semiconductor Electrodes and Dye-Sensitized Solar Cells. *J. Phys. Chem. B* **2004**, *108*, 2323−2332.
(36) Fabregat-Santiago, F.; Garcia-Belmonte, G.; Mora-Sero, I.; Bisquert, J. Characterization of Nanostructured Hybrid and Organic Solar Cells by Impedance Spectroscopy. *Phys. Chem. Chem. Phys.* **2011**, *13*, 9083−9118.
(37) Bisquert, J.; Marcus, R. A. Device Modeling of Dye-Sensitized Solar Cells. *Top. Curr. Chem.* **2013**, *352*, 325−395.
(38) Bisquert, J. Fractional Diffusion in the Multiple-Trapping Regime and Revision of the Equivalence with the Continuous-Time Random Walk. *Phys. Rev. Lett.* **2003**, *91*, 010602.
(39) Kopidakis, N.; Benkstein, K. D.; van de Lagemaat, J.; Frank, A. J. Transport-Limited Recombination of Photocarriers in Dye-Sensitized Nanocrystalline TiO_2 Solar Cells. *J. Phys. Chem. B* **2003**, *107*, 11307−11315.
(40) Wang, Q.; Zhang, Z. P.; Zakeeruddin, S. M.; Gratzel, M. Enhancement of the Performance of Dye-Sensitized Solar Cell by Formation of Shallow Transport Levels under Visible Light Illumination. *J. Phys. Chem. C* **2008**, *112*, 7084−7092.
(41) Cass, M. J.; Qiu, F. L.; Walker, A. B.; Fisher, A. C.; Peter, L. M. Influence of Grain Morphology on Electron Transport in Dye Sensitized Nanocrystalline Solar Cells. *J. Phys. Chem. B* **2003**, *107*, 113−119.
(42) Park, K.; Zhang, Q.; Myers, D.; Cao, G. Charge Transport Properties in TiO_2 Network with Different Particle Sizes for Dye Sensitized Solar Cells. *ACS Appl. Mater. Interfaces* **2013**, *5*, 1044−1052.
(43) Bisquert, J.; Vikhrenko, V. S. Interpretation of the Time Constants Measured by Kinetic Techniques in Nanostructured Semiconductor Electrodes and Dye-Sensitized Solar Cells. *J. Phys. Chem. B* **2004**, *108*, 2313−2322.
(44) Hagfeldt, A.; Grätzel, M. Light-Induced Redox Reactions in Nanocrystalline Systems. *Chem. Rev.* **1995**, *95*, 49−68.
(45) Gregg, B. A.; Pichot, F.; Ferrere, S.; Fields, C. L. Interfacial Recombination Processes in Dye-Sensitized Solar Cells and Methods to Passivate the Interfaces. *J. Phys. Chem. B* **2001**, *105*, 1422−1429.
(46) Snaith, H. J.; Grätzel, M. The Role of a "Schottky Barrier" at an Electron-Collection Electrode in Solid-State Dye-Sensitized Solar Cells. *Adv. Mater.* **2006**, *18*, 1910−1914.
(47) Bisquert, J.; Mora-Sero, I.; Fabregat-Santiago, F. Diffusion-Recombination Impedance Model for Solar Cells with Disorder and Nonlinear Recombination. *ChemElectroChem* **2013**, *1*, 289−296.
(48) Ansari-Rad, M.; Abdi, Y.; Arzi, E. Reaction Order and Ideality Factor in Dye-Sensitized Nanocrystalline Solar Cells: A Theoretical Investigation. *J. Phys. Chem. C* **2012**, *116*, 10867−10872.
(49) Raga, S. R.; Barea, E. M.; Fabregat-Santiago, F. Analysis of the Origin of Open Circuit Voltage in Dye Solar Cells. *J. Phys. Chem. Lett.* **2012**, *3*, 1629−1634.
(50) Kern, R.; Sastrawan, R.; Ferber, J.; Stangl, R.; Luther, J. Modeling and Interpretation of Electrical Impedance Spectra of Dye Solar Cells Operated under Open-Circuit Conditions. *Electrochim. Acta* **2002**, *47*, 4213−4225.

DOI: 10.1021/am506101z
ACS Appl. Mater. Interfaces 2015, 7, 1100−1106